Hall magnetohydrodynamics in a strong magnetic field

Daniel O. Gómez,[1,a)] Swadesh M. Mahajan,[2] and Pablo Dmitruk[1]
[1]*Departamento de Física, Facultad de Ciencias Exactas y Naturales, Universidad de Buenos Aires, Ciudad Universitaria, 1428 Buenos Aires, Argentina*
[2]*Institute for Fusion Studies, The University of Texas, Austin, Texas 78712, USA*

(Received 27 May 2008; accepted 8 September 2008; published online 7 October 2008)

For a plasma embedded in a strong external magnetic field, the spatial structures tend to develop fine scales preferentially across the field, rather than along the parallel direction. This feature, which allowed a major simplification in the theoretical structure of one-fluid magnetohydrodynamics (leading to reduced magnetohydrodynamics), is exploited here to derive what may be called the reduced Hall magnetohydrodynamic equations (RHMHD) reflecting two-fluid effects such as the Hall current and the electron pressure. These physical effects, which can be relevant in astrophysical environments and also in fusion plasmas, allow for the propagation of circularly polarized normal modes such as whistlers and shear/ion-cyclotron waves. In this paper, the RHMHD system of equations is integrated numerically, to investigate externally driven turbulence. © *2008 American Institute of Physics*. [DOI: 10.1063/1.2991395]

I. INTRODUCTION

One-fluid magnetohydrodynamics (MHD) is often regarded as a reasonable description of the large-scale dynamics of a plasma. A first step toward a more appropriate theory for fully ionized plasmas is to consider two-fluid effects through a generalized Ohm's law which includes the Hall current. Whenever one deals with phenomena with characteristic length scales comparable or smaller than the ion skin depth c/ω_i (c: speed of light; ω_i: ion plasma frequency), the Hall effect cannot be neglected. Among its other manifestations, the Hall current causes (in an ideal plasma) the magnetic field to become frozen in the electron flow instead of being carried along with the bulk velocity field. Another important feature of the ideal Hall-MHD description is the self-consistent presence of parallel (i.e., to the magnetic field) electric fields, which can therefore accelerate particles. Hall-MHD has recently been invoked in advancing our understanding of phenomena ranging from dynamo mechanisms,[1] magnetic reconnection,[2–4] and accretion[5,6] to the physics of turbulent regimes.[7–10]

In many cases of interest, such as in fusion devices or astrophysical plasmas, a strong externally supported magnetic field is present. This external field breaks the isotropy of the problem and can be responsible of important changes in the dynamics, such as in reconnection regimes or in the development of energy cascades in turbulent systems. For one-fluid MHD, the existence of a strong magnetic field is often exploited to yield a simpler model: the so-called reduced MHD approximation (RMHD; see Refs. 11 and 27). In this approximation, the fast compressional Alfvén mode is eliminated, while the shear Alfvén and the slow magnetosonic modes are retained.[12] The RMHD equations have been used to investigate a variety of problems such as current sheet formation,[13,14] nonstationary reconnection,[15,16] the dynamics of coronal loops,[17,18] or the development of turbulence.[19] The self-consistency of the RMHD approximation has been analyzed in Ref. 20. Moreover, recent numerical simulations have studied the validity of the RMHD equations by directly comparing its predictions with the compressible MHD equations in a turbulent regime.[21]

In this paper we derive the asymptotic equivalent of the Hall-MHD equations; the resulting set will describe the slow dynamics of plasmas (with Hall currents) embedded in a strong external magnetic field and will naturally include new features such as the presence of parallel electric fields. We organize the paper as follows. After introducing the Hall-MHD set of equations in Sec. II, we perform the asymptotic expansion corresponding to the dynamics of a plasma embedded in a strong external magnetic field in Sec. III, and derive the set of equations that could be called reduced Hall-MHD (RHMHD). The linear modes of RHMHD are displayed in Sec. IV. The results obtained from the numerical integration of the complete dynamic equations are presented in Sec. V, while in Sec. VI we summarize our conclusions.

II. THE HALL-MHD SYSTEM

The equations of motion of an ideal fully ionized plasma, made of an ion species of particle mass m_i and electrons of negligible mass (since $m_e \ll m_i$) are given by[22]

$$m_i n \frac{d\boldsymbol{U}}{dt} = en\left(\boldsymbol{E} + \frac{1}{c}\boldsymbol{U} \times \boldsymbol{B}\right) - \nabla p_i, \tag{1}$$

$$0 = -en\left(\boldsymbol{E} + \frac{1}{c}\boldsymbol{U}_e \times \boldsymbol{B}\right) - \nabla p_e, \tag{2}$$

where $\boldsymbol{U}, \boldsymbol{U}_e$ are the ion and electron flow velocities, respectively, and $\boldsymbol{E}, \boldsymbol{B}$ are the electric and magnetic fields, respectively. The electron and ion pressures p_e, p_i are assumed to satisfy polytropic laws

$$p_i \propto n^{\gamma}, \tag{3}$$

a)Also at Instituto de Astronomía y Física del Espacio, C. Universitaria, 1428 Buenos Aires, Argentina. Electronic mail: dgomez@df.uba.ar.

$$p_e \propto n_e^{\gamma}. \tag{4}$$

Charge neutrality and mass conservation add $n_i = n_e = n$ and

$$\frac{\partial(m_i n)}{\partial t} + \nabla \cdot (m_i n \boldsymbol{U}) = 0 \tag{5}$$

to the system, while the Ampère's law ($\boldsymbol{J}$ is the current)

$$\boldsymbol{J} = \frac{c}{4\pi} \nabla \times \boldsymbol{B} = en(\boldsymbol{U} - \boldsymbol{U}_e) \tag{6}$$

closes the system. The electric and magnetic fields can be expressed in terms of the electrostatic potential ϕ and the vector potential $\boldsymbol{A}$ as

$$\boldsymbol{E} = -\frac{1}{c}\partial_t \boldsymbol{A} - \nabla \phi \tag{7}$$

and

$$\boldsymbol{B} = \nabla \times \boldsymbol{A}. \tag{8}$$

The preceding set of equations can be cast in a dimensionless form in terms of a typical longitudinal length scale L_0, an ambient density $n = n_0$, a typical value for the magnetic field B_0, a typical velocity corresponding to the Alfvén speed $v_A = B_0/\sqrt{4\pi m_i n_0}$, and reference pressures p_0 and p_{0e},

$$\frac{d\boldsymbol{U}}{dt} = \frac{1}{\epsilon}(\boldsymbol{E} + \boldsymbol{U} \times \boldsymbol{B}) - \beta \nabla p_i, \tag{9}$$

$$0 = -\frac{1}{\epsilon}(\boldsymbol{E} + \boldsymbol{U}_e \times \boldsymbol{B}) - \beta \nabla p_e, \tag{10}$$

and

$$\boldsymbol{J} = \nabla \times \boldsymbol{B} = \frac{1}{\epsilon}(\boldsymbol{U} - \boldsymbol{U}_e), \tag{11}$$

where we have introduced the Hall parameter

$$\epsilon = \frac{c}{\omega_i L_0} = \sqrt{\frac{m_i c^2}{4\pi e^2 n_0 L_0^2}} \tag{12}$$

and the plasma *beta*

$$\beta = \frac{p_0}{m_i n_0 v_A^2}. \tag{13}$$

By adding Eqs, (9) and (10), and by eliminating $\boldsymbol{E}$ and $\boldsymbol{U}_e$ in Eq, (10), we derive the equivalent pair consisting of the plasma equations of motion (9) and (10)

$$\frac{d\boldsymbol{U}}{dt} = (\nabla \times \boldsymbol{B}) \times \boldsymbol{B} - \beta \nabla (p_i + p_e), \tag{14}$$

and the Ohm's law equations (7)–(11) into Eqs. (10); i.e.,

$$\partial_t \boldsymbol{A} = (\boldsymbol{U} - \epsilon \nabla \times \boldsymbol{B}) \times \boldsymbol{B} - \nabla \phi + \epsilon \beta \nabla p_e. \tag{15}$$

Equations (14) and (15) constitute what may be called the ideal Hall-MHD (HMHD) equations. The HMHD system has been thoroughly studied, both analytically and numerically. It is possible to obtain several important general results by manipulation of Eqs. (14) and (15), but detailed numerical calculations are somewhat difficult with the full raw system, particularly in the presence of a strong external magnetic field which forces the parallel and perpendicular dynamics to be at different spatial scales. The existence of a strong external field, however, can be exploited to simplify or reduce the system. This spirit, epitomized in reduced MHD (RMHD), is precisely our guide here when we seek an appropriate and consistent procedure to reduce HMHD to what might be termed "RHMHD."

III. HALL-MHD IN A STRONG MAGNETIC FIELD

The presence of a strong external magnetic field forces spatial structures to develop fine-scale structure across the external field, without changing their parallel size appreciably.[23–26] Let as assume, for instance, that the normalized magnetic field is of the form (the external field is along $\hat{\boldsymbol{e}}_z$)

$$\boldsymbol{B} = \hat{\boldsymbol{e}}_z + \delta \boldsymbol{B}, \quad |\delta \boldsymbol{B}| \approx \alpha \ll 1, \tag{16}$$

where α represents the typical tilt of magnetic field lines with respect to the $\hat{\boldsymbol{e}}_z$ direction. Therefore, as for reduced MHD, one expects

$$\nabla_\perp \approx 1, \quad \partial_z \approx \alpha \ll 1. \tag{17}$$

To guarantee that the vector fields $\boldsymbol{B}$ and $\boldsymbol{U}$ remain solenoidal (incompressible flow), we decompose them as

$$\boldsymbol{B} = \hat{\boldsymbol{e}}_z + \nabla \times (a\hat{\boldsymbol{e}}_z + g\hat{\boldsymbol{e}}_x) \tag{18}$$

and

$$\boldsymbol{U} = \nabla \times (\varphi \hat{\boldsymbol{e}}_z + f\hat{\boldsymbol{e}}_x), \tag{19}$$

where the potentials $a(\boldsymbol{r},t)$, $g(\boldsymbol{r},t)$, $\varphi(\boldsymbol{r},t)$, and $f(\boldsymbol{r},t)$ are all assumed of order $\alpha \ll 1$.

Notice that the potentials f and g are usually neglected in reduced MHD applications and simulations, and that the potentials a and φ restrict the dynamics to velocity and magnetic field components perpendicular to the external magnetic field. The potentials $f \neq 0 \neq g$ allow nonzero dynamical field components along $\hat{\boldsymbol{e}}_z$. These parallel components are actually retained in standard RMHD theory,[27] giving rise passive scalar equations for the field components along $\hat{\boldsymbol{e}}_z$. In Hall-MHD, it is essential to retain the potentials f and g, to capture the helical behavior introduced by the Hall terms; i.e., those proportional to ϵ in Eq. (15).

Assuming also $\partial_t \approx \alpha \ll 1$, we obtain, to first order in α in Eqs. (14) and (15),

$$\nabla_\perp [\partial_y g - \beta(p_i + p_e)] = 0, \tag{20}$$

$$\nabla_\perp [\phi + \varphi + \epsilon(\partial_y g - \beta p_e)] = 0, \tag{21}$$

which are the Bernoulli conditions constraining the pressures and the electrostatic potential.

To order α^2, Eqs. (14) and (15) describe the dynamical evolution of the potentials (i.e., a, φ, g, and f),

$$\partial_t a = \partial_z(\varphi - \epsilon b) + [\varphi - \epsilon b, a], \tag{22}$$

$$\partial_t \omega = \partial_z j + [\varphi, \omega] - [a, j], \tag{23}$$

$$\partial_t b = \partial_z(u - \epsilon j) + [\varphi, b] + [u - \epsilon j, a], \tag{24}$$

$$\partial_t u = \partial_z b + [\varphi, u] - [a, b], \tag{25}$$

where $j=-\nabla_\perp^2 a$ and $\omega=-\nabla_\perp^2 \varphi$ are, respectively, the parallel current and vorticity components, and $[a,b]=\partial_x a \partial_y b - \partial_y a \partial_x b$ indicate the standard Poisson brackets. The parallel component of the dynamical magnetic field is $b=-\partial_y g$, and that of the velocity field is $u=-\partial_y f$. Both of these components are usually assumed to be zero in reduced MHD applications and simulations. However, in standard RMHD theory they are retained and passive scalar equations are obtained for the parallel components (see Ref. 27). Note that Eqs. (24) and (25) are indeed passive scalar equations for u and b for the case $\epsilon=0$.

Equations (22)–(25) together with the Bernoulli conditions

$$b + \beta(p_i + p_e) = \text{const}, \tag{26}$$

$$\phi + \varphi - \epsilon(b + \beta p_e) = \text{const} \tag{27}$$

describe the dynamical evolution of an incompressible Hall plasma embedded in a strong external magnetic field. In analogy with MHD, we call this system the reduced HMHD (RHMHD). The derivation of the RHMHD is one of the main goals of this paper. In the next section (Sec. IV) we derive the linear modes that RHMHD can sustain, and in Sec. V we show typical numerical solutions of the nonlinear evolution equations.

Just as for three-dimensional Hall-MHD, this set of equations display three ideal invariants: the energy

$$E = \frac{1}{2}\int d^3r(|\boldsymbol{U}|^2 + |\boldsymbol{B}|^2)$$

$$= \frac{1}{2}\int d^3r(|\nabla_\perp \varphi|^2 + |\nabla_\perp a|^2 + u^2 + b^2), \tag{28}$$

the magnetic helicity

$$H_m = \frac{1}{2}\int d^3r(\boldsymbol{A}\cdot\boldsymbol{B}) = \int d^3r ab, \tag{29}$$

and the hybrid helicity[28,29]

$$H_h = \frac{1}{2}\int d^3r(\boldsymbol{A} + \epsilon\boldsymbol{U})\cdot(\boldsymbol{B} + \epsilon\boldsymbol{\Omega})$$

$$= \int d^3r[\ ab + \epsilon(a\omega + ub) + \epsilon^2 u\omega)], \tag{30}$$

where $\boldsymbol{\Omega}=\nabla\times\boldsymbol{U}$ is the vorticity vector field.

IV. LINEAR MODES IN HALL-MHD

Retaining only the linear terms in Eqs. (22)–(25) and considering all variables to behave like $\exp[i\boldsymbol{k}_\perp\cdot\boldsymbol{r}_\perp + ik_z z - i\sigma t]$, we readily obtain the following dispersion relationship:

$$\sigma^4 - 2k_z^2\left[1 + \tfrac{1}{2}(\epsilon k_\perp)^2\right]\sigma^2 + k_z^4 = 0, \tag{31}$$

yielding the normal modes

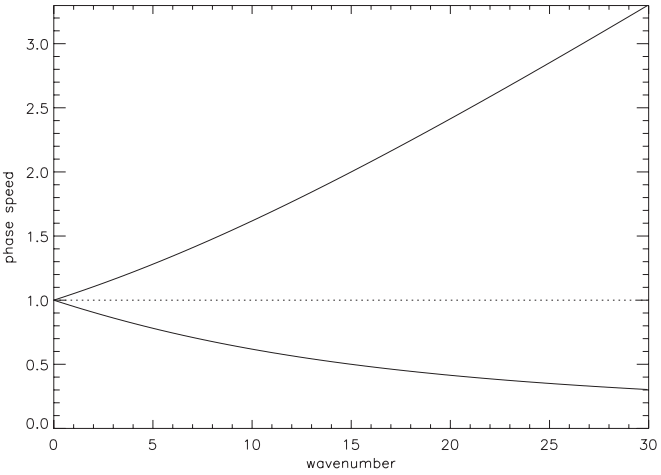

FIG. 1. The phase speed σ/k_z vs perpendicular wavenumber (i.e., $|\boldsymbol{k}_\perp|$) is displayed for the two branches. The whistler branch grows monotonically, while the shear ion-cyclotron mode has monotonically decreasing phase speed with wavenumber. The unsplit Alfvén mode, which is the only one present in the limit $\epsilon=0$, is shown with a dotted trace for reference.

$$\sigma_\pm = \sqrt{k_z^2 + \left(\frac{\epsilon k_\perp k_z}{2}\right)^2} \pm \frac{\epsilon k_\perp k_z}{2}. \tag{32}$$

The positive branch (σ_+) corresponds to the *whistler* mode, while the negative branch σ_- represents shear ion-cyclotron waves. The variation of the phase speed σ/k_z for these modes as a function of $|\boldsymbol{k}_\perp|$ is shown in Fig. 1. Naturally, for $\epsilon=0$, the only residual mode is the dispersionless shear Alfvén wave.

V. NUMERICAL INTEGRATION OF THE HALL-MHD EQUATIONS

We integrate Eqs. (22)–(25) numerically, assuming periodicity for the lateral boundary conditions, and specifying the velocity fields at the boundaries ($z=0$ and $z=L$). The particular boundary motions considered for this paper, are $\varphi(z=0)=0$, while $\varphi(z=L)$ is a superposition of Fourier modes $\boldsymbol{k}$ such that $3\leqslant|\boldsymbol{k}|\leqslant 4$ (for a detailed description, see Ref. 19). The details of these boundary motions are not relevant; what is important is that they pump energy into the system and drive it into a turbulent regime. For the spatial derivatives on the (x,y) plane, we use a pseudo-spectral technique with de-aliasing, while finite differences are adopted for the (much smoother) $\hat{\boldsymbol{e}}_z$ derivatives. Since the system is being driven from the boundaries, we start all our simulations with trivial initial conditions (i.e., $a=\varphi=u=b=0$).

To study the role of the Hall current in a plasma permeated by a strong magnetic field, we performed a set of simulations with different values of the Hall parameter (namely, $\epsilon=0,\ 0.031,\ 0.062,\ 0.125$). The size of all these simulations is $256\times256\times30$. In Fig. 2, we show the ratio of total kinetic energy (i.e., for both parallel and perpendicular motions) to total energy (i.e., kinetic plus magnetic). For pure MHD ($\epsilon=0$), this ratio is about $E_{\text{tot}}^{\text{kin}}/E_{\text{tot}}\approx0.057$. For the same parameters, we find that as the Hall parameter ϵ rises, the kinetic fraction increases, becoming as high as $E_{\text{tot}}^{\text{kin}}/E_{\text{tot}}\approx0.123$ for $\epsilon=0.125$ (see Fig. 2).

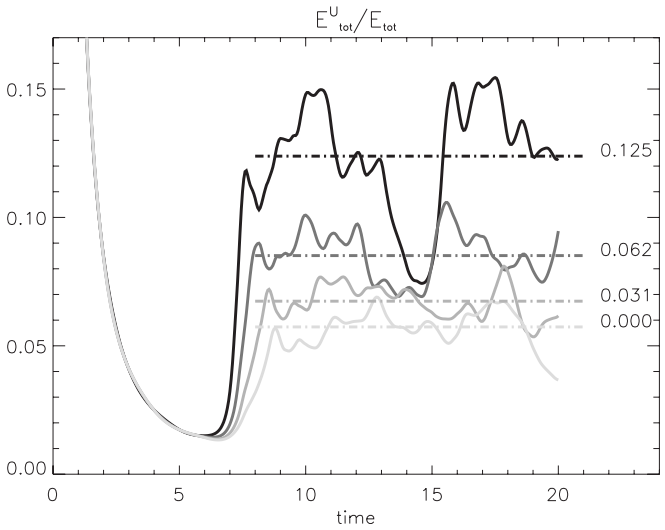

FIG. 2. Ratio of total kinetic energy to total energy vs time for different values of the Hall parameter ϵ (labeled).

In the MHD limit ($\epsilon=0$), the total energy reduces to [Eq. (28)]

$$E_{\mathrm{perp}} = \frac{1}{2}\int d^3r(|\nabla_\perp \varphi|^2 + |\nabla_\perp a|^2), \tag{33}$$

while for the general case ($\epsilon \neq 0$), there is a fraction of the total energy directly associated with the parallel degrees of freedom:

$$E_{\mathrm{par}} = \frac{1}{2}\int d^3r(u^2 + b^2). \tag{34}$$

The fraction $E_{\mathrm{par}}/E_{\mathrm{tot}}$ is displayed in Fig. 3 for different values of the Hall parameter ϵ. Note that for all these cases, parallel fluctuations become non-negligible only after times of the order of $t \approx 6-8$. This timescale is not directly controlled by the external driver (which is feeding only the perpendicular components in a stationary fashion); it is the typical time it takes to the perpendicular part of the dynamics to ignite parallel fluctuations via terms proportional to ϵ in Eq. (24). For a moderate value $\epsilon=0.125$, we find that the parallel dynamics can store up to 7.5% of the total energy. Fluctuations of this energy ratio also become proportionally larger, since it is only the total energy that remains invariant.

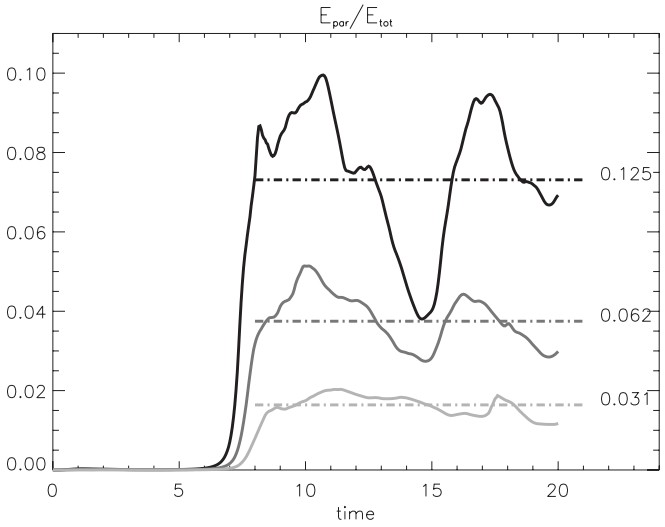

FIG. 3. Ratio of parallel energy (kinetic plus magnetic) to total energy for different values of the Hall parameter ϵ (labeled).

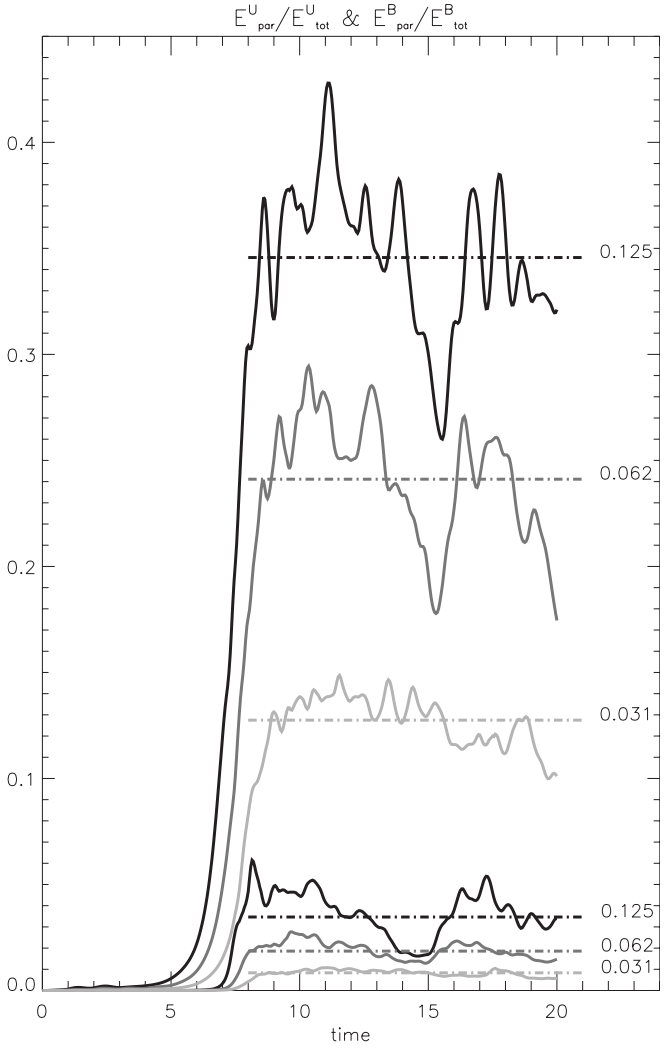

FIG. 4. Ratios of parallel to total magnetic and kinetic energies for different values of the Hall parameter ϵ (labeled). The three upper curves correspond to magnetic energy ratios, while the lower curves correspond to kinetic energy ratios.

In Fig. 4 we display the detail of how the energy splits into parallel and perpendicular degrees of freedom, and also into the kinetic and the magnetic energies, for different values of ϵ. In Fig. 2 we have already seen that, although the fraction of kinetic energy grows with ϵ, most of the energy in our simulations is magnetic. In Fig. 4 we see that for $\epsilon=0.125$, up to 34.5% of the magnetic energy is associated with the parallel dynamics, while only 3.8% of the kinetic energy is associated to parallel flows.

The Hall effect is expected to affect the dynamics of patterns whose sizes are of the order of the ion skin depth (i.e., c/w_{pi}) or smaller. According to Eq. (12), this typical size is $\lambda \approx \epsilon L_0$. In Fourier space, it corresponds to a typical wavenumber $k_\epsilon = 1/\epsilon$. In Figs. 5 and 6 we show the spectral

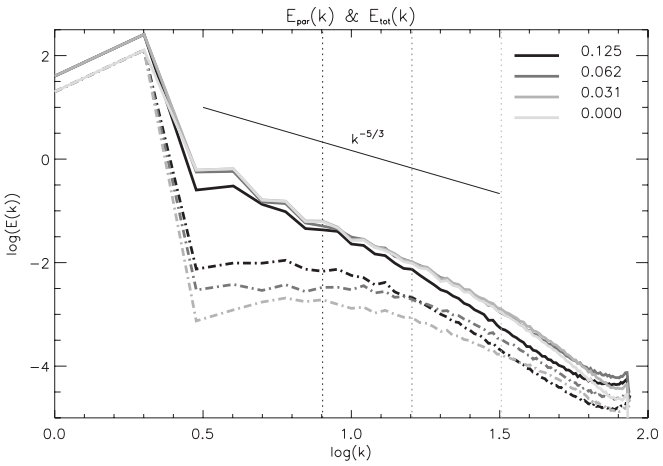

FIG. 5. Energy power spectrum for different values of the Hall parameter ϵ (labeled) at $t=20$. Full traces correspond to total energy, and the Kolmogorov slope is displayed for reference. Dot-dashed traces correspond to just the parallel part of the total energy. Vertical dashed lines indicate the location of $k_\epsilon=1/\epsilon$ for the values of ϵ considered.

distribution of energy corresponding to $t=20$. We remind the reader that the time unit is L_0/v_A (i.e., the Alfvén time along the main magnetic field) and that the system reaches a stationary regime by $t\approx 8$, as shown, for instance, in Fig. 2. Bold lines in both figures correspond to the total energy power spectra for different values of the Hall parameter ϵ. Even though our numerical simulations have only a moderate spatial resolution, the energy spectra are not inconsistent with the slope predicted by Kolmogorov in what could be interpreted as the inertial range. Figure 5 also shows the spectra for the parallel part of energy in dot-dashed traces. For each of the simulations, characterized by a given value of ϵ, we find that the parallel energy spectrum becomes a fair fraction of the total energy spectrum for $k \geqslant k_\epsilon$. In Fig. 6 we show the power spectra for kinetic energy in dot-dashed trace. Even though in these simulations kinetic and magnetic energy do not reach equipartition, kinetic energy spectra reach a sizeable fraction of the total for $k \geqslant k_\epsilon$.

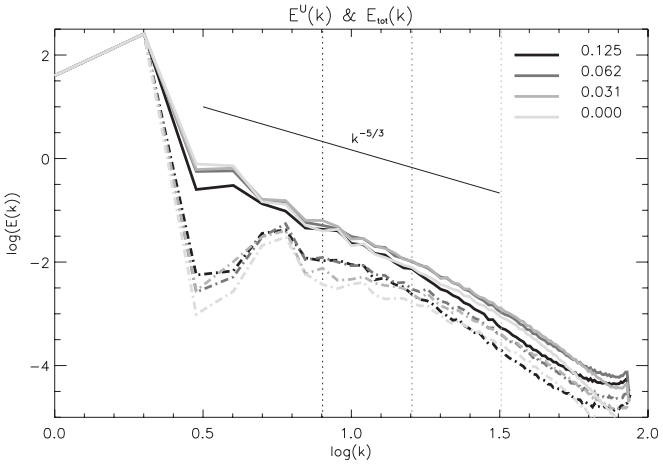

FIG. 6. Energy power spectrum for different values of the Hall parameter ϵ (labeled) at $t=20$. Full traces correspond to total energy (same as Fig. 5). Dot-dashed traces correspond to kinetic energy. Vertical dashed lines indicate the location of $k_\epsilon=1/\epsilon$ for the values of ϵ considered.

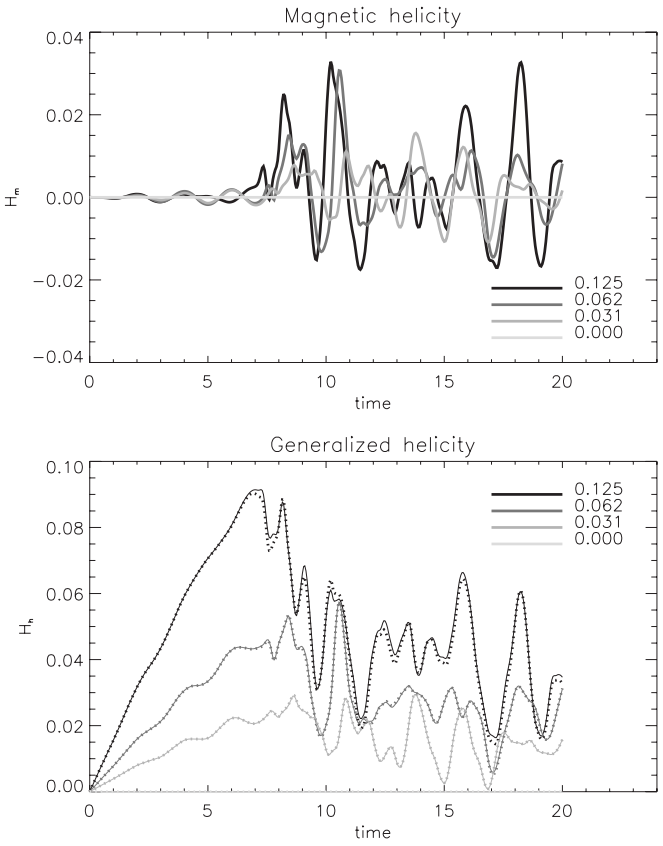

FIG. 7. The upper panel shows magnetic helicity vs time [$H_m(t)$; see Eq. (29)] for different values of the Hall parameter ϵ (labeled). The lower panel shows hybrid helicity vs time [$H_h(t)$, see Eq. (30)] for different values of the Hall parameter ϵ (labeled). The dotted traces correspond to the approximate expression given in Eq. (36).

The behavior of both the magnetic and the hybrid helicity can be seen in Fig. 7. The upper panel shows the magnetic helicity as a function of time for different values of the parameter ϵ. For $\epsilon=0$ (RMHD), the magnetic helicity is trivially zero, and does not enter the dynamics at all. When $\epsilon \neq 0$, however, the magnetic helicity oscillates around zero in all the cases considered. Even though the amplitude of these oscillations grow with ϵ, when averaged in time, the system tends not to store magnetic helicity. The lower panel in Fig. 7 shows the hybrid helicity as a function of time for different values of the parameter ϵ. The hybrid helicity for the case $\epsilon=0$ is also trivially zero, since it coincides with the magnetic helicity in this asymptotic limit. However, for $\epsilon \neq 0$, the hybrid helicity is stored in the system with a net sign (positive, in this case). We also plotted an approximate expression of the hybrid helicity, using a dotted trace. The reason for the good fit between the full and dotted curves stems from the fact that according to Eq. (30), for sufficiently small ϵ, is

$$H_h \approx H_m + \epsilon K, \tag{35}$$

where

$$K = \frac{1}{2}\int d^3 r \boldsymbol{U}\cdot\boldsymbol{B} = \int d^3 r (a\omega + ub) \tag{36}$$

is the so-called cross-helicity. The cross-helicity is one of the ideal invariants (along with energy and magnetic helicity) in plain MHD, but not in Hall-MHD.

VI. CONCLUSIONS

In this paper we have derived the basic equations which comprise the new system of reduced Hall-MHD (RHMHD) following the asymptotic procedure used in deriving the conventional RMHD. The derived system describes the slow dynamics of Hall plasmas embedded in a strong external magnetic field. The larger RHMHD subsumes RMHD and contains additional physics such as the existence of parallel electric fields, and normal modes like whistlers and shear/ion-cyclotron waves.

This asymptotic low-frequency limit defining RHMHD equations is described by two solenoidal vector fields (the velocity and magnetic fields), which are generated by four scalar fields. In RMHD, on the other hand, only two scalar fields are needed (namely, the stream function and the magnetic flux), from which the velocity and magnetic vector fields perpendicular to the external magnetic field may be derived. In the more general four scalar description [see Eqs. (22)–(25)], both vector fields are allowed parallel components as well, and therefore can fully display the helical nature of the dynamics induced by the Hall effect.

We checked that the reduced model is still capable of sustaining the whistler and shear/ion-cyclotron modes of the full Hall-MHD. Since the shear/ion-cyclotron phase speed is a decreasing function of wavenumber, its associated electric field can be potentially relevant in accelerating and heating particles. This feature of Hall plasmas is, of course, well known; we only emphasize that it is retained in the geometrically simple model presented here.

We also report the results of a set of numerical simulations with different values of the Hall parameter, to study changes in the plasma dynamics as the Hall effect becomes progressively more important. We find, for instance, that as ϵ is raised, both the kinetic energy and the fraction of the total energy entertained in the parallel degrees of freedom, are boosted up. We find that these two features (relative importance of kinetic energy versus magnetic energy and relative importance of parallel energy versus perpendicular energy) are much more noticeable at small spatial scales, in particular, whenever $k \geqslant k_\epsilon$, as shown Figs. 5 and 6. These figures also show that the power spectrum displayed in the stationary turbulent regime is not inconsistent with a Kolmogorov power-law, as it is also the case for RMHD.[19] However, simulations at a considerably larger spatial resolution are required to derive a reliable value for the slope.

In summary, we report the derivation of a theoretical model which describes the slow dynamics of a Hall plasma embedded in a strong magnetic field. We believe that this model will be potentially quite useful for a number of applications such as fusion devices and astrophysical plasmas.

ACKNOWLEDGMENTS

Research of S.M.M. was supported by US DOE Contract No. DE-FG03-96ER-54366. D.O.G. and P.D. are members of the Carrera del Investigador Científico of CONICET, and their research has been partially funded by Grant Nos. X092/08 and X429/08 from the University of Buenos Aires and by Grant No. PICT 33370/05 from ANPCyT.

[1] P. D. Mininni, D. O. Gómez, and S. M. Mahajan, Astrophys. J. **584**, 1120 (2003).
[2] F. Mozer, S. Bale, and T. D. Phan, Phys. Rev. Lett. **89**, 015002 (2002).
[3] D. Smith, S. Ghosh, P. Dmitruk, and W. H. Matthaeus, Geophys. Res. Lett. **31**, 02805, DOI: 10.1029/2003GL018689 (2004).
[4] L. F. Morales, S. Dasso, and D. O. Gómez, J. Geophys. Res. **110**, A04204, DOI: 10.1029/2004JA010675 (2005).
[5] M. Wardle, Mon. Not. R. Astron. Soc. **303**, 239 (1999).
[6] S. A. Balbus and C. Terquem, Astrophys. J. **552**, 235 (2001).
[7] W. H. Matthaeus, P. Dmitruk, D. Smith, S. Ghosh, and S. Oughton, Geophys. Res. Lett. **30**, 2104, DOI: 10.1029/2003GL017949 (2003).
[8] P. D. Mininni, D. O. Gómez, and S. M. Mahajan, Astrophys. J. **619**, 1019 (2005).
[9] S. Galtier, J. Plasma Phys. **72**, 721 (2006).
[10] P. Dmitruk and W. H. Matthaeus, Phys. Plasmas **13**, 2307 (2006).
[11] H. Strauss, Phys. Fluids **19**, 134 (1976).
[12] G. P. Zank and W. H. Matthaeus, J. Plasma Phys. **48**, 85 (1992).
[13] A. A. van Ballegooijen, Astrophys. J. **311**, 1001 (1986).
[14] D. W. Longcope, and R. N. Sudan, Astrophys. J. **437**, 491 (1994).
[15] D. L. Hendrix and G. van Hoven, Astrophys. J. **467**, 887 (1996).
[16] L. Milano, P. Dmitruk, C. H. Mandrini, D. O. Gómez, and P. Demoulin, Astrophys. J. **521**, 889 (1999).
[17] D. O. Gómez and C. Ferro Fontán, Astrophys. J. **394**, 662 (1992).
[18] P. Dmitruk and D. O. Gómez, Astrophys. J. Lett. **527**, L63 (1999).
[19] P. Dmitruk, D. O. Gómez, and W. H. Matthaeus, Phys. Plasmas **10**, 3584 (2003).
[20] S. Oughton, P. Dmitruk, and W. H. Matthaeus, Phys. Plasmas **11**, 2214 (2004).
[21] P. Dmitruk, W. H. Matthaeus, and S. Oughton, Phys. Plasmas **12**, 112304 (2005).
[22] N. A. Krall and A. W. Trivelpiece, in *Principles of Plasma Physics* (McGraw-Hill, New York, 1973), p. 89.
[23] J. V. Shebalin, W. H. Matthaeus, and D. Montgomery, J. Plasma Phys. **29**, 525 (1983).
[24] S. Oughton, E. R. Priest, and W. H. Matthaeus, J. Fluid Mech. **280**, 95 (1994).
[25] W. H. Matthaeus, S. Oughton, S. Ghosh, and M. Hossain, Phys. Rev. Lett. **81**, 2056 (1998).
[26] S. Oughton, W. H. Matthaeus, and S. Ghosh, Phys. Plasmas **5**, 4235 (1998).
[27] D. C. Montgomery, Phys. Scr. **T2/1**, 83 (1982).
[28] L. Turner, IEEE Trans. Plasma Sci. **PS14**, 849 (1983).
[29] S. M. Mahajan and Z. Yoshida, Phys. Plasmas **7**, 635 (2000).